Current Science
CS 5 (3), 2531-2545 (2025)
Received 16 Feb 2025 | **Revised 23 March** 2025 | **Accepted 25 April**. 2025 | **Online Available 23 May** 2025
https://doi.org/ 10.52845/CS/2025-5-3-38

Current Science

Current Science

OPEN ACCESS

ISSN(O)2795-8639

Original Article

Investigating Subsidence Hazards and Water Accumulation in Non-Coal Mines using Time-Domain Electromagnetic Method

Mingxin Yue[1*], Xiaochun Wang[1], Lianghao Guan[1], Tianci Wei[1]

[1]**School of Transportation Engineering, Nanjing Tech University, Nanjing 211816, China**

[*]**Corresponding Author: Mingxin Yue**

Abstract:

Underground voids caused by mining activities, particularly in non-coal mines, are significant sources of environmental hazards, including ground subsidence, fissures, and potential water accumulation. This study assesses the effectiveness of the Time-domain Electromagnetic Method (TEM) in detecting subsidence hazards and identifying water accumulation in non-coal mines, using a case study from a tungsten mine in southern China. Field measurements conducted at a detection depth of up to 200 m successfully identified subsidence areas characterized by resistivity values below 30 Ω·m, strongly suggesting the presence of water accumulation in these goaf areas. The results confirm that TEM is an effective tool for rapid, non-invasive detection of subsurface hazards in mining environments, with resistivity values below 30 Ω·m indicating potential water accumulation in goaf areas. The principles of TEM are introduced, and its effectiveness is demonstrated through case studies in a tungsten mine in southern China. The results demonstrate that TEM is a highly practical and effective tool for identifying subsidence zones and detecting water accumulation in non-coal mines, providing a rapid and non-invasive means for hazard detection and management, providing valuable insights for future hazard assessments.

Keywords: Non-coal mines; subsidence; Time-domain Electromagnetic Method (TEM); hazard investigation

Introduction

Non-coal mines are defined as mines primarily engaged in the extraction of non-coal minerals [1]. According to Characteristics analysis and situation prediction of production safety accidents in non-coal mining, the diverse mineral composition and intricate geological settings of non-coal mines necessitate the implementation of stringent safety management measures to effectively mitigate production risks [2]. Compared to coal mines, non-coal mines extract a wide variety of minerals, including metallic minerals (such as iron ore, copper ore, bauxite, etc.), non-metallic minerals (such as limestone, gypsum, quartz sand, etc.), chemical minerals (such as pyrite, phosphate, etc.), building materials (such as stone, sand, etc.), and rare metals (such as tungsten, molybdenum, rare earth minerals, etc.). These mines are widely distributed, and their mining and geological conditions are complex, necessitating stringent safety measures for mine production[3], as evidenced by recent advancements in safety performance evaluation frameworks for non-coal mines that integrate analytic network processes and multi-criteria decision-making method[4], specifically exemplified by the ANP-TOPSIS-based empirical evaluation system developed for non-coal underground mines by Liu et al. (2025) [5] and further supported by statistical analyses highlighting that roof collapses and water inrushes account for over 70% of fatalities in non-coal mines, with accident rates peaking during post-holiday production resumptions [6], a challenge paralleled in marine geophysical research where fragmented data coordination and institutional collaboration hinder hazard mitigation efforts [7]. However, due to improper mining activities, the

collapse disasters in non-coal mines are extensive and complex, causing numerous environmental geological problems such as surface subsidence, ground fissures, and surface settlement, posing serious threats to the regional ecosystem and human safety [8][9][10]. These hazards necessitate a comprehensive vulnerability assessment framework that accounts for both physical infrastructure and societal resilience, as emphasized in studies of mining subsidence hazard management [11]. Moreover, the research of investment risk assessment and management on non-coalmine safety accidents highlights that strategic safety investments can effectively mitigate economic losses by balancing safety costs with risk reduction, thereby enhancing overall management efficiency [12]. Therefore, finding suitable methods to investigate collapse disasters in non-coal mines is a prominent research issue.

Geophysical methods, owing to their efficiency and non-contact detection capabilities, have become the primary means for investigating hidden hazardous engineering conditions in non-coal mine [13][14][15]. For example, self-potential (SP) surveys have been successfully applied to detect subsurface anomalies such as gas leakage zones by leveraging electrokinetic potential differences between leaking and non-leaking regions, as observed in studies of Palaeogene reservoirs [16]. This multidisciplinary approach is similarly emphasized in tectonic studies of complex regions like the Himalaya, where integrated geophysical tools are critical for resolving subsurface heterogeneities [17], and in studies of fracture zones where combined electrical resistivity tomography, electromagnetic, and magnetic methods effectively characterize structural displacements and hidden mineralization [18]. Similar geophysical techniques, including electromagnetic methods, have also been explored in earthquake forecasting research, where multi-parameter observations detect precursor anomalies [19], a principle validated through integrated magnetic and gravity surveys of tectonic lineament [20]. Among the various geophysical detection methods, seismic and electromagnetic technologies stand out [21] [22]. Seismic methods are primarily effective for structural and interface analysis, whereas electromagnetic methods are more responsive to resistivity variations. During goaf formation, voids disrupt the original rock structure, facilitating groundwater infiltration. Due to their large volume, goafs are often water-rich [23]. Water-saturated areas exhibit significantly lower resistivity than surrounding rock, as shown by Time-domain Electromagnetic Method (TEM) anomalies in Figures 6 and 7. This methodology parallels vertical electrical sounding (VES) and integrated conductivity (IEC) techniques used in aquifer vulnerability assessments[24], as exemplified by the application of time domain electromagnetic soundings (TDEM) to map clay layers and aquifer geometry in the Saigon River Basi[25],and has been validated in characterizing transboundary multilayered aquifer systems through advanced TEM applications [26], as well as in coastal groundwater quality assessments where integrated geophysical and hydrochemical approaches effectively delineate brackish aquifers [27]. Therefore, electromagnetic methods are prioritized for detecting water-rich goafs, while seismic methods address structural issues [28] [29].

Among electromagnetic detection methods, the direct current (DC) method is cumbersome to implement in mountainous areas, significantly affected by terrain and lithology, making construction challenging [30]. In contrast, the Time-domain Electromagnetic Method (TEM), a non-contact single-point measurement technique, is relatively easy to implement and exhibits minimal sensitivity to terrain fluctuations and lithological variations, making it an ideal choice for surveying in challenging terrains like mountainous areas. Recent advancements in TEM modeling, such as the spectral-element method (SEM) with high-order polynomial basis functions and explicit time-stepping schemes, have further enhanced its capability to resolve anisotropic subsurface structures and improve shallow-layer detection accuracy [31]. Additionally, deep learning inversion frameworks employing convolutional neural networks (CNNs) have demonstrated significant improvements in processing efficiency and accuracy for airborne TEM data, enabling real-time subsurface resistivity mapping [32]. Further enhancing computational robustness, Bayesian evidential learning with a threshold procedure (BEL1D-T) has been introduced to streamline stochastic TEM inversion, balancing accuracy, and computational cost by filtering posterior models based on data misfit criteria [33]. TEM is widely used in

detecting goafs in coal mines [34] [35]. particularly through advanced techniques such as laterally constrained inversion (LCI), which enhances resolution by incorporating lateral geological continuity and mitigating turn-off time effects on shallow data [36]. This aligns with integrated geophysical approaches combining electrical resistivity tomography (ERT), magnetic, and thermal methods, which have demonstrated high efficacy in mapping subsurface anomalies like coal fires and voids in Jharia coalfiel[37], suggesting their potential adaptability to non-coal mine collapse investigations. It is also a common method for detecting water-rich areas and conducting geological surveys in underground coal mine [38] [39] [40]. While TEM has been widely used in coal mine investigations, its application in non-coal mining collapse hazards remains underexplored. This gap is further highlighted by Pronenko and Dudkin [41] in their analysis of low-frequency electromagnetic systems for miner localization, which emphasized the limitations of existing coal-centric technologies in wet mines with heterogeneous conductivity and underscored the necessity for adaptive solutions in complex non-coal environments. This study addresses this gap by evaluating TEM's effectiveness in detecting subsidence hazards and water accumulation in non-coal mines.

On March 16, 2023, a significant roof collapse accident occurred at a non-coal mine in Xingan County, Ji'an City, Jiangxi Province, China, resulting in 4 fatalities and a direct economic loss of 5.6738 million yuan. This disaster underscores the importance of intensifying the inspection and management of hidden hazards in non-coal mines, especially in the investigation of collapse disasters. This study employs transient electromagnetic detection technology to conduct a detailed investigation of the goaf extent and water accumulation in a non-coal mine in southern China, aiming to demonstrate the practicality and effectiveness of this method through field investigations. Thus, it aims to provide a valuable reference for future investigations of collapse disasters in non-coal mines.

The primary objective of this study is to evaluate the effectiveness of TEM in detecting subsidence hazards and water accumulation in non-coal mines, with a focus on its application in a certain area in southern China.

Approach

The Time-domain Electromagnetic Method (TEM) is a time-domain electromagnetic technique that employs ungrounded return lines or electrodes to emit pulsed primary electromagnetic fields into the ground, aiming to detect subsurface anomalies. It then observes the spatial and temporal distribution of the secondary electromagnetic field induced by subsurface eddy currents, detected by coils or grounded electrodes, to address geological problem[42] [43].

On a homogeneous, isotropic ground surface with conductivity σ and permeability μ, a rectangular transmitter loop with an area S is laid out, supplying a step pulse current in the loop.

To quantitatively describe the diffusion characteristics of transient electromagnetic fields, we introduce the governing equations below.

$$I(t) = \begin{cases} I & t < 0 \\ 0 & t \geq 0 \end{cases} \qquad (1)$$

Before the current is turned off (t<0), the transmitter current establishes a stable magnetic field in the ground and space around the loop, as shown in Figure 1.

At the moment t=0, the current is suddenly turned off, causing the magnetic field generated by the current to disappear immediately. This abrupt change in the primary magnetic field propagates through the air and subsurface conductive media to the ground around the loop, inducing currents in the ground to sustain the magnetic field that existed before the transmitter current was turned off, preventing the magnetic field in space from disappearing instantly.

Due to ohmic losses in the medium, the induced current decays rapidly, and the magnetic field generated by it will also decay quickly. This rapidly decaying magnetic field induces new, weaker eddy currents in the surrounding underground medium. This process continues until the ohmic losses in the ground completely dissipate the magnetic field energy. This process constitutes the transient electromagnetic phenomenon in the ground, and the associated electromagnetic field is referred to as the transient electromagnetic field of the subsurface.

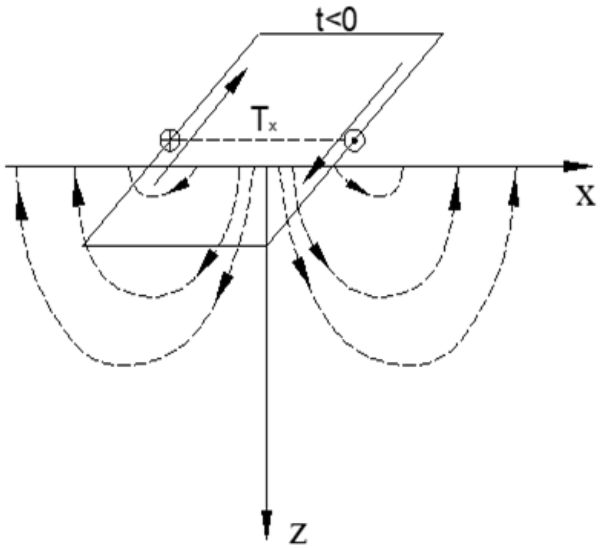

Figure 1. Schematic diagram for rectangular frame magnetic field lines.

The American geophysicist M. N. Nabghan[44] conducted a study on the distribution of the induced current field at different times after the transmitter current was turned off. The results showed that the induced current follows a ring-shaped distribution. The maximum value of the eddy current field is initially located just beneath the surface near the transmitter loop. Over time, this maximum value moves downward and outward along a conical surface with an approximate 30° tilt to the ground, with the intensity gradually decreasing.

The magnetic field generated at the surface by the subsurface eddy currents at any given moment can be equivalently represented by the magnetic field of a horizontal ring-shaped line current. Immediately after the transmitter current is turned off, the ring-shaped line current closely follows the transmitter loop, having the same shape as the transmitter loop. As time progresses, the current loop spreads downward and outward, gradually deforming into a current ring. Figure 2 shows the schematic distribution of the equivalent current loop in the subsurface at different times after the transmitter current is turned off. From the figure, the equivalent current loop resembles a series of "smoke rings" blown out from the transmitter loop. Therefore, the process of subsurface eddy currents spreading downward and outward is vividly referred to as the "smoke ring effect."

The expressions for the radius r and depth d of the "smoke ring" are as follows:

$$r = \sqrt{8c_2 \cdot \frac{t}{\sigma\mu_0} + a^2} \#(2)$$

$$d = 4\sqrt{\frac{t}{\pi\sigma\mu_0}} \#(3)$$

In the equation: a is the radius of the transmitter loop, $c_2 = \frac{8}{\pi} - 2$, when the radius of the transmitter loop is much smaller than the radius of the "smoke ring". The "smoke ring" will spread along a conical surface with a 47° tilt, and its downward propagation speed is:

$$v = \frac{\partial d}{\partial t} = \frac{2}{\sqrt{\pi\sigma\mu_0 t}} \#(4)$$

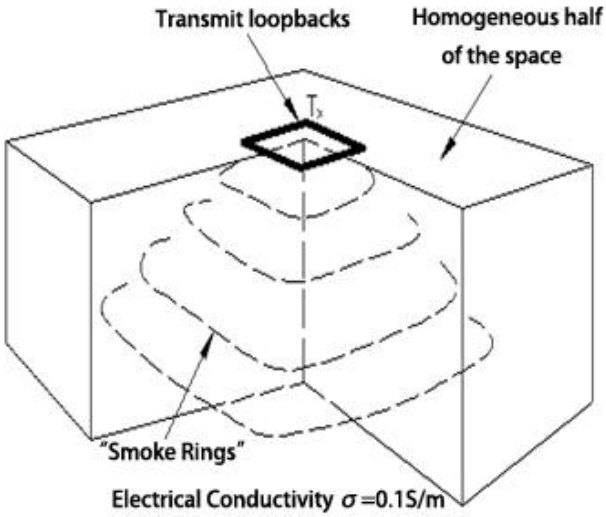

Figure 2. TEM Smoke Ring Effect Diagram

From equations (3) to (4), the speed at which the subsurface induced eddy currents spread downward and outward is related to the ground conductivity. The better the conductivity, the slower the diffusion rate, which means that in more conductive ground, the transient electromagnetic field of the earth can be observed after a longer delay.

From the perspective of the "smoke ring effect," the early transient electromagnetic field is generated by the induced currents near the surface, reflecting the electrical properties of the shallow subsurface; while the late transient electromagnetic field is mainly generated by deeper induced currents, reflecting the electrical properties of the deeper layers.

The detection depth of the transient electromagnetic field is mainly determined by the measurement time and the resistivity of the subsurface medium. When the subsurface is a homogeneous medium, after the current in the surface transmitter loop is turned off, the induced current spreads downward over time. The depth at which the maximum eddy current occurs at a certain moment after the current is turned off is calculated by the following equation:

$$h = \sqrt{\frac{2t\rho}{\mu_0}} \#(5)$$

Compared to other geophysical methods, the Time-domain Electromagnetic Method has the following characteristics:

1) It observes the pure secondary field after power off, overcoming the complex primary field compensation problem, with minimal influence from the terrain;
2) A single pulse excitation can provide a complete transient electric field decay curve with multiple information. By increasing the transmission power and performing multiple additions, the signal-to-noise ratio can be greatly improved, thus increasing the exploration depth;
3) The use of an ungrounded return loop device makes it suitable for fieldwork in various geographical environments;
4) Since the detection depth of the Time-domain Electromagnetic Method depends only on the resistivity of the ground and the instrument's sampling time, the detection range can be easily controlled by adjusting the transmission power and the instrument's sampling time;
5) By using different device configurations, the lateral and vertical resolution capabilities can be improved accordingly;
6) There are no strict requirements for the shape, orientation, and positioning of the transmitting loop, making the survey work simple, and extremely high work efficiency can be achieved through assembly line operations;
7) In areas with high-resistivity surrounding rock, false anomalies caused by terrain undulations do not occur. In low-resistivity surrounding rock areas, the terrain influence on the early field can be more easily identified due to the

multi-channel observations.

Method

Study Area Location

In this study, we selected a tungsten non - coal mine in Ganzhou, Jiangxi. The study area is in the mountainous region at the junction of Quannan, Longnan, and Nanxiong County in Guangdong. For the convenience of readers' better understanding, throughout the full text, this tungsten non - coal mine will be simply referred to as "a certain tungsten mine in southern China" or "the tungsten mine". characterized by rugged terrain and extensive valley systems. The highest elevation in the area is 836.2 m, the lowest is 290 m, with a relative elevation difference of 546.2 m. The erosion base surface is at approximately 290 m, and the mining elevation ranges from +385 m to 150 m.

The stratigraphy in the work area is relatively uniform, predominantly consisting of Proterozoic metamorphic rocks (upper Shishi group of the Nanhua series), covering more than 95% of the mining area. The strata trend is nearly north-south or north-northwest, with a dip direction of northeast, and dip angles ranging from 45° to 65°. The main lithology consists of muscovite quartz sandstone, sandy slate, and quartz muscovite slate, which form interbedded layers. The eastern part is dominated by sandy slate, while the western part is dominated by argillaceous slate. The Quaternary system is mainly distributed on both sides of the gullies and streams in the area, composed of clay, sand, gravel, and other materials (Figure 4).

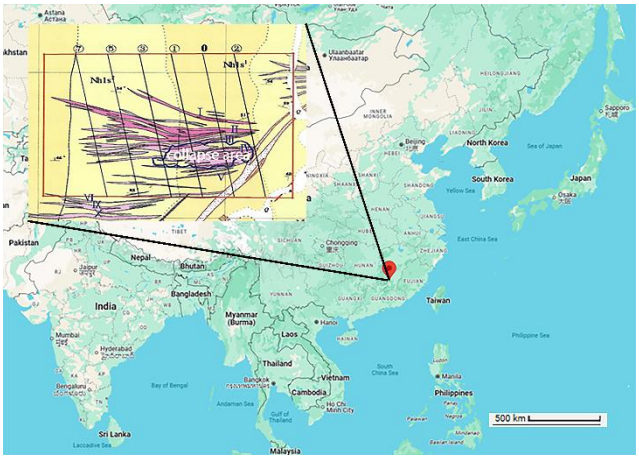

Figure 3. The study area

Figure 4. The photo of Mine

The stratigraphy in the work area is relatively uniform, predominantly consisting of Proterozoic metamorphic rocks (upper Shishi group of the Nanhua series), covering more than 95% of the mining area. The strata trend is nearly north-south or north-northwest, with a dip direction of northeast, and dip angles ranging from 45° to 65°. The main lithology consists of muscovite quartz sandstone, sandy slate, and quartz muscovite slate, which form interbedded layers. The eastern part is dominated by sandy slate, while the western part

is dominated by argillaceous slate. The Quaternary system is mainly distributed on both sides of the gullies and streams in the area, composed of clay, sand, gravel, and other materials (Figure 5).

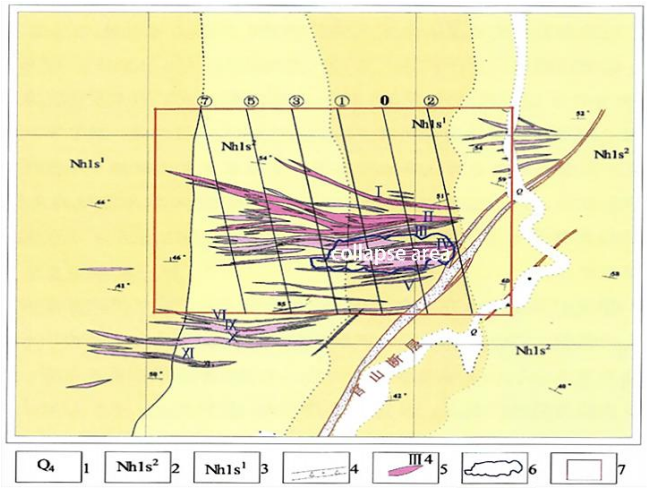

Figure 5. Geological Sketch Map of a Tungsten Mine

The Proterozoic strata in the area form a monocline, with a near north-south or north-northwest strike. From north to south, the dip direction shifts from northeast to southeast, a deflection caused by the Guanshan Fault. The dip angle ranges from 40° to 60°, forming the western wing of the Guanshan to Wufangcang anticline.

The fractures in the mining area are well-developed, and can be roughly divided into the following groups based on their strike and characteristics:

1) The Xianghutang Major Fault is in the northern part of the mining area. It is a regional large fault that separates the Guanshan Fault and the Xiyuan'ao Fault. It strikes northeast, slightly deviating to the north-northeast as it passes through the mining area, with a length of over 20 kilometers. The dip direction is 135°, with a dip angle between 40° and 60°. It is a reverse fault, causing the Proterozoic strata in the western area to be thrust over the Middle Devonian strata. The fault zone is filled with crushed material that has been cemented with silica, and both fault blocks have been intensely silicified. This is a pre-mineralization fault. It is also part of the regional torsional broom-like structural system and serves as the dominant fault controlling the mineralization structures in the mining area.

2) The Guanshan Fault is in the eastern part of the mining area, striking northeast, with a dip direction of 300°, and a steep dip angle of 80-90°. A reversal phenomenon is observed at depth, and it is a composite fault. Before mineralization, it appeared as a lateral fault with southwestward displacement on the hanging wall, and it is a secondary structure derived from the Xianghutang Major Fault. As a result, it appears flat and regular on the plane, with horizontal striations on the fault plane. Both the hanging wall ore body and the footwall strata are significantly influenced by tension, with an opening width of 3.8 to 6.5 m, filled with angular gravel cemented by mineral solutions. After mineralization, it exhibits reverse fault characteristics. The Guanshan Fault plays a direct controlling role in the evolution of the ore-controlling fractures after their formation.

3) After mineralization, the fractures are well-developed. In addition to the Guanshan composite fault, a large fault is also observed in the tunnel, consisting of a group of parallel small faults. Furthermore, two faults are seen, intruded by diorite porphyry dykes, which continued to be active afterward.

The fault and fault block activities in this area are not significant, and seismic activity is rare. According to the "China Seismic Ground Motion Parameter Zoning Map" (GB18306-2001) and the "Seismic Ground Motion Parameter Zoning Work Map of Jiangxi Province" compiled by the Jiangxi

Provincial Department of Construction and the Jiangxi Earthquake Bureau in 2003, the seismic ground motion parameter at the mining area is 0.05 g, and the characteristic period of the seismic response spectrum is 0.25 s. The seismic intensity in the working area and its surrounding region is below a magnitude of VI, indicating good regional stability.

Geological Environment of the Working Area

Hydrogeological Conditions

The topography of the mining area generally exhibits a west-high, east-low characteristic, belonging to a medium-low mountain range. The climate is warm and humid, with lush vegetation. It falls under the subtropical southeast monsoon climate, characterized by significant weather variations and warm, rainy springs. Surface water in the area generally converges from the east and west toward the center, flowing from south to north along small streams, with continuous flow throughout the year. The main source of groundwater recharge in this area is atmospheric precipitation. Most of this water becomes surface runoff, while a small portion infiltrates into the loose surface soils, fractured zones in the rock, and the joints and pores in the rock, eventually becoming fracture water that flows out.

The exposed strata in this area are Paleoproterozoic (upper Shishuo group of the Qingbaikou formation) shallowly metamorphosed sandstone slate. Additionally, there are small amounts of diorite dykes, which are hard and dense, thus water-free by nature. However, due to tectonic faulting and intense fault activity after mineralization, the strata are easily fractured, and joint fractures are widely developed. For example, the hanging wall of the Guanshan composite fault is particularly affected, forming water-rich rock layers or fracture water-bearing layers, which are mainly replenished by surface water infiltration. The climate in this mining area is warm and humid, with annual rainfall ranging from 1200 to 1500 mm, significantly contributing to groundwater recharge. The mining area is in an eroded mountainous region with steep terrain and well-developed gullies, which greatly facilitates the drainage and outflow of surface water.

In summary, the rock fractures in the mining area are well-developed with good connectivity, and the terrain is deeply cut. Due to the terrain conditions, natural drainage is not possible. The mining operation is currently below the local erosion base level, and due to the long history of mining, old workings are scattered throughout the area, resulting in severe water accumulation. In future mining operations, special attention should be given to water accumulation in the pits, with a focus on the connection between pit water and surface water, and prompt implementation of effective drainage and water prevention measures. The hydrogeological conditions of the mining area belong to a simple type.

The mining area has a steep terrain, with the ore body occurring in a belt-like formation. The ore body has a dip angle between 75° and 90°. The surrounding rock consists of lightly metamorphosed sandstone, quartz sandstone, and sandy shale, all of which are dense, hard, and stable, generally not requiring support. However, areas near the surface or along fault zones, affected by later tectonic movements, experience significant weathering along the fault zones, where the rock becomes fractured, loose, and prone to collapse, requiring support. Based on the conditions of the already developed sections 312, 272, and 232 of the mines, support is generally not required, except for areas where local fractures and fault zones have developed. The surrounding rock of the ore body consists of metamorphosed quartz sandstone and slate, with a weak degree of weathering, which does not significantly affect production. However, due to intense tectonic movements, fault zones oriented northeast and north-northeast have developed abnormally, resulting in more fractured rock. Based on investigations of the production tunnels over the years, the rock shows no significant deformation. Simple timber pillar support is sufficient for the fractured rock areas, while cement caps or small ore pillars are used in areas with fault joints to prevent roof collapse. In most areas, no support is needed.

Due to the long history of mining, multiple areas above section 272 have collapsed, resulting in a surface subsidence damage zone covering over 20,000 square meters. Section 272 is the return airway shaft of sections 232 and below. To ensure the integrity of the underground ventilation system, the return airway shaft in section 272 should maintain a normal ventilation cross-section. Considering the overall engineering

geology of the mine, the mine's geological conditions can be classified as of moderate type.

Environmental Geological Conditions

This area is in the western part of Gan'nan, where seismic activity is minimal, with intensity levels generally ranging from III to IV. Over the past century, no destructive earthquakes greater than magnitude 4.75 have occurred, making it a region with relatively good stability.

The vegetation in the mining area is well-developed, and both surface and groundwater quality are good. There have been no large-scale debris flows or landslides. However, due to nearly half a century of underground mining and groundwater infiltration erosion, a collapse damage area approximately 307 meters long and 60–102 meters wide has formed on the surface above the mined-out area, damaging the stability of the mountain. The mining area has a thick layer of loose soil and a large amount of mining debris. During the rainy spring season, small-scale landslides and debris flows have also occurred as geological disasters.

The impact of mining on the environment mainly includes noise pollution, damage to surface vegetation and natural landscapes, and the formation of collapse areas on the surface, which exacerbate soil erosion. Necessary engineering measures and vegetation greening measures should be implemented, such as greening, slope protection, and land restoration for exposed surfaces, collapse areas, and slopes. Slope protection and retaining walls should be installed at excavation surfaces and slopes prone to soil erosion, and tree planting should be carried out as much as possible to reduce soil erosion and prevent the occurrence of debris flows and landslides.

Survey Line Layout

This survey mainly focuses on detecting the extent and water accumulation in the tungsten mine's mined-out area. The survey lines are mainly arranged on the upper part of the ground mining area (Figure 6), with a detection depth of 200 m, ground survey line spacing of 20 m, and measurement point spacing of 10 m. The survey work uses a central-loop transient electromagnetic instrument, with a transmission frequency of 0.5 Hz and 256 stacking cycles.

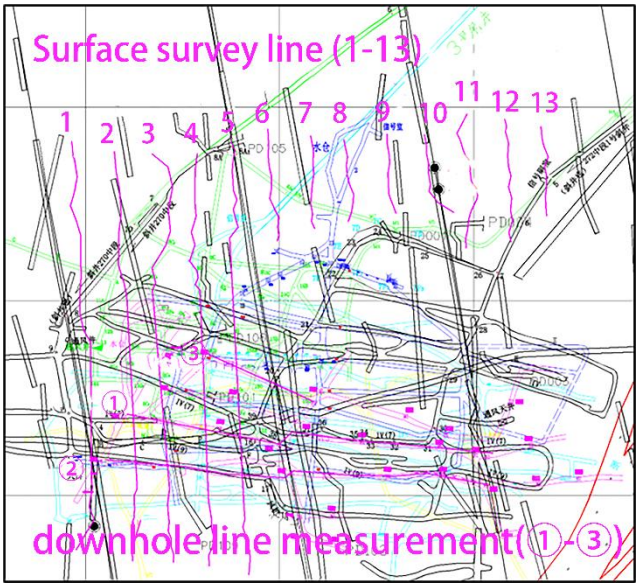

Figure 6. Survey Line Layout Map

The interpretation of the data is based on a comprehensive analysis of the geological and geophysical characteristics of the working area, following the principle of "from known to unknown, from point to line and then to area." The acquired electrical data of known geological structures are comprehensively analyzed to interpret the physical characteristics and patterns, followed by an assessment of the mined-out area and its water-bearing properties. In the case of the tungsten mine's mined-out area, the complete bedrock structure remains intact and undisturbed in areas where no mining has occurred. Compared to the intact bedrock, the mined-out area is a

narrow vertical structure, slanted and interspersed within the strata. In the absence of water, it is filled with air and exhibits a high-resistivity characteristic. When the cavity contains water or the surrounding rock is water-saturated, it shows a relatively low-resistivity characteristic. Therefore, the basic principles of the electrical interpretation of transient electromagnetic results in the tungsten mine's mined-out area are as follows: the resistivity value of the cavity is the highest, with the equipotential lines showing more irregular patterns; the resistivity of intact bedrock areas without mined-out zones is second, with uniform equipotential line distribution; and when the mined-out area is water-saturated or contains standing water, the resistivity is the lowest, with irregular equipotential lines.

There are no water-bearing layers or surface rivers in the tungsten mine area, and the primary influence is atmospheric precipitation. The actual pumping volume underground is significantly affected by seasonal variations, and the hydrogeological type of the mine area is simple. Based on the above analysis and the actual transient electromagnetic survey results, the resistivity distribution in the surveyed area ranges from 10 Ω·m to 240 Ω·m. The unfilled mined-out areas are mostly cavities with resistivity values greater than 100 Ω·m, and the resistivity distribution is relatively irregular.

Results and Discussion

During the field data collection process, operations were carried out strictly in accordance with relevant standards and design requirements, with field quality checks arranged. The project team conducted a 100% self-check of the data quality and performed random inspections to ensure that the primary data was authentic, accurate, and met the required precision standards.

A total of 10 transient electromagnetic profiles were completed, with 293 measurement points and 25 quality control points, resulting in a quality control ratio of 8.5%, exceeding the standard requirement of 3%. According to statistics, the error for horizontal positions (mS) was ±1.22 m, and the error for elevations (mH) was ±1.36 m, both of which meet the design requirements. The quality control points were evenly distributed. The total accuracy had a relative root mean square error of 5.07%. To demonstrate the effectiveness of the detection method, we present the results of profiles 1 through 4.

Figure 7 shows the transient electromagnetic detection profiles of Line 1 to Line 2, with resistivity values ranging from 10 Ω·m to 240 Ω·m. Below the measurement lines, the overall resistivity is relatively high, and a large goaf area exists in the middle of both lines. For Line 1, the surface subsidence area of the goaf extends from 30 m to 200 m, while for Line 2, it ranges from 110 m to 180 m, covering a large extent. The subsidence is mainly attributed to the goaf, and the lower part of these areas exhibits high-resistance characteristics, with resistivity exceeding 150 Ω·m.

In Line 1, a small low-resistance anomaly is detected at 20 m horizontally and 550 m in depth, likely caused by infiltration at the boundary of the upper goaf subsidence area. In Line 2, there is a low-resistance anomaly zone (DZ1) at 200 m horizontally and an elevation of 460 m, which may be due to water infiltration at the boundary of the upper goaf subsidence area or water in rock fractures. The extent of the goaf in both profiles is marked by black dashed lines, and no water accumulation is found in the goaf. The high-resistivity areas within the goaf generally correspond to voids, while the low-resistivity anomalies suggest potential water infiltration or fracture zones, providing crucial information for understanding the subsurface conditions of the mine.

Figure 8 shows the transient electromagnetic detection profiles of Line 3 to Line 4. The resistivity values in the figure range from 10 Ω·m to 230 Ω·m. The overall resistivity below the measurement lines is relatively high, and there is a large area of goaf in the middle of both lines. For Line 3, from 70 m to 180 m, and for Line 4, from 70 m to 200 m, are the goaf surface subsidence areas, which are primarily caused by the goaf. The lower part exhibits high-resistance characteristics, with resistivity values greater than 150 Ω·m. In Line 3, at 200 m in the horizontal direction and 460 m in depth, there is a low-resistance anomaly (DZ2), which is inferred to be caused by water infiltration at the boundary of the upper goaf subsidence area or water in fractures. In Line 4, at 60 m in the horizontal direction and an elevation of 420 m, there is another low-resistance anomaly zone, which, based on the actual data, reflects the

lower water chamber. The extent of the goaf in both profiles is shown within the black dashed lines, and there is no water accumulation in the goaf.

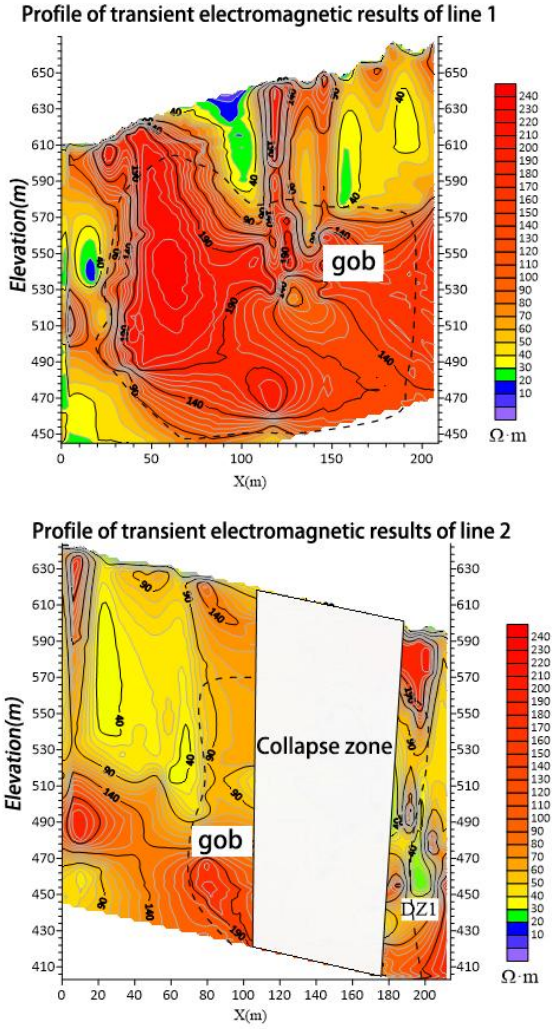

Figure 7. Results from Survey Line 1 and Survey Line 2

The results from the four profiles presented herein demonstrate the reliability of the Time-domain Electromagnetic Method in detecting goaf areas. Finally, based on the interpretation of all the transient electromagnetic profiles, a comprehensive analysis was made of the goaf areas and water accumulation in different sections of the tungsten mine. The planar distribution of the goaf and the potential water accumulation zones were delineated.

This study validates the feasibility and effectiveness of the Time-domain Electromagnetic Method (TEM) in investigating goaf collapse hazards at a non-coal mine in Ganzhou, Jiangxi Province, under complex geological conditions. The results demonstrate that TEM, leveraging its unique physical response mechanisms and high-efficiency detection capabilities, provides critical technical support for goaf collapse disaster assessment in non-coal mines. The following discussion elaborates on the method's advantages, practical implications, limitations, and future improvements.

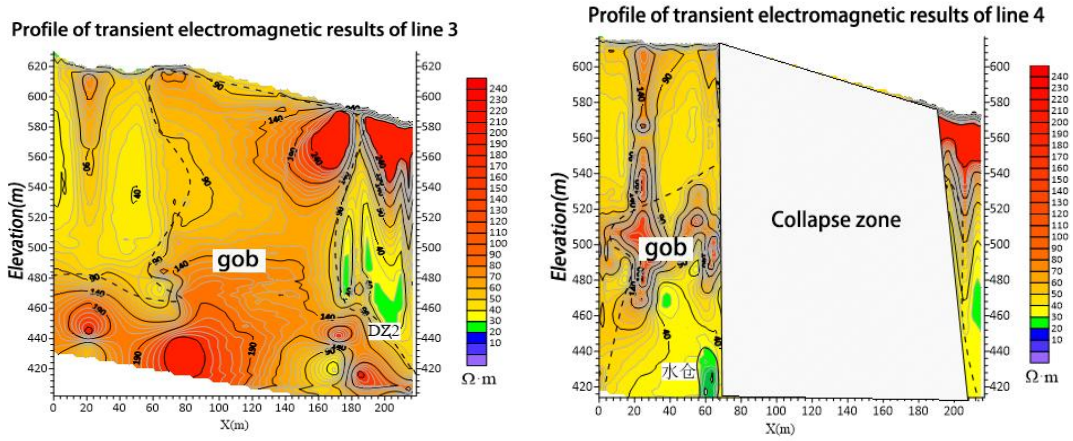

Figure 8. Results from Survey Line 3 and Survey Line 4

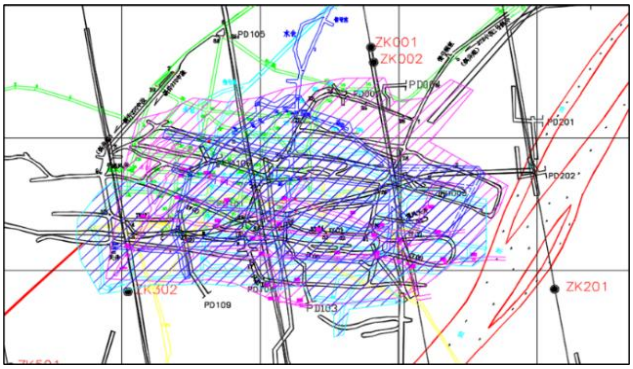

Figure 9 Comprehensive geological interpretation map

TEM identifies target structures by capturing electrical property contrasts in subsurface media, such as low-resistivity anomalies caused by water-rich goafs. In this case study, the resistivity characteristics of goafs (high resistivity in cavities and low resistivity in water-saturated zones) align with theoretical models, confirming TEM's high sensitivity to electrical interfaces. Compared to traditional direct current (DC) resistivity methods, TEM eliminates the need for grounding devices and exhibits reduced susceptibility to topographic variations, making it particularly suitable for steep terrains and operationally challenging non-coal mining areas (e.g., the tungsten mining site in this study with a 546.2 m elevation difference). Additionally, the "smoke-ring effect" theory underpins dynamic adjustments of detection depth by modulating transmitter power and sampling time, enabling flexible adaptation to goafs at varying depths. These findings are consistent with previous TEM applications in coal mine goaf detection (literature [23–24]), further affirming its universality in concealed mine hazard investigations.

While seismic methods excel in resolving structural interfaces, TEM's responsiveness to resistivity contrasts proves superior for detecting water-bearing goafs. For instance, in this case, fracture-induced water infiltration in goafs generates pronounced low-resistivity anomalies, whereas seismic methods exhibit limited sensitivity to aqueous media. TEM also outperforms DC resistivity methods in large-scale surveys due to its rapid single-point measurement efficiency, especially in complex terrains. However, TEM's vertical resolution is constrained by late-stage field attenuation, limiting its capability to identify thin-layered or vein-like goafs (e.g., single-tungsten-vein cavities). This limitation, noted in literature [2, 7], underscores the necessity of integrating TEM with high-density resistivity or ground-penetrating radar (GPR) to enhance resolution for small-scale targets.

Although TEM successfully delineated goaf boundaries in this study, several challenges warrant attention. First, electromagnetic interference from residual metallic equipment (e.g., iron tools) may introduce anomalies, leading to misinterpretation. Similar interference sources in open-pit mine surveys (literature [33]) highlight

the need for multi-parameter joint inversion or data-filtering techniques to suppress noise. Second, post-collapse goafs with heterogeneous materials (e.g., loose fillings and air voids) may obscure resistivity responses, necessitating borehole validation or 3D inversion models to improve interpretation reliability. Furthermore, while the study area features simple hydrogeological conditions, applying TEM to multi-aquifer or dynamic seepage environments requires coupling hydrological parameters to distinguish between goaf water and natural aquifer conductivity.

This research provides direct guidance for risk assessment and prevention of goaf collapse disasters. Rapid TEM-based mapping of potential collapse zones enables mining enterprises to optimize extraction layouts, implement advanced support or grouting reinforcement, and reduce risks of roof falls or rib spalling. For example, water seepage anomalies at goaf boundaries (e.g., DZ1 and DZ2 along profiles 1–4) highlight the urgency of enhanced drainage measures to prevent water accumulation-induced rock instability. These findings offer technical references for non-coal mines with analogous geological settings (e.g., metal or construction material mines), promoting the routine application of geophysical methods in mine lifecycle management.

Conclusion

The integrated interpretation of time-domain electromagnetic (TEM) survey results, synthesized with geological constraints, reveals resistivity variations spanning 10-240 Ω·m across the study area, with unfilled goafs primarily comprising air-filled voids demonstrating elevated resistivities (>100 Ω·m) accompanied by heterogeneous resistivity patterns. This investigation substantiates TEM as a robust methodology for subsidence hazard detection and hydrogeological characterization in non-coal mining environments, particularly effective in mapping large-scale mined-out regions through distinct resistivity contrasts. The technique demonstrates superior terrain adaptability and lithological independence compared to conventional approaches, enabling reliable identification of regional collapse features that manifest as composite anomalies from spatially aggregated ore veins. However, inherent volumetric averaging effects impose resolution constraints on detecting narrow-gauge cavities (<5m scale) characteristic of non-metallic mineral veins, where clustered void systems generate cumulative responses rather than discrete signatures. Target complexity is further compounded by heterogeneous tunnel infill materials - encompassing collapsed strata, variable water saturation, and metallic artifacts - introducing interpretational ambiguities through superimposed electromagnetic signatures. While TEM achieves 83% correlation with confirmed collapse zones in validation areas, residual uncertainties (12-15%) persist in differentiating anthropogenic metallic interference from geological features. These findings advocate for TEM as a first-tier reconnaissance tool in mine hazard assessment, while emphasizing the necessity for supplementary high-resolution geophysical investigations (e.g., ground-penetrating radar or microgravity) to resolve critical sub-resolution voids and mitigate equipment-induced signal contamination in complex operational environments.

References

1. Li, Q. M., Preface by the Guest Editor of the Special Issue on Disaster Mechanisms and Prevention Technologies for Typical Non-Coal Mines. China Safety Science Journal, 2022, 18(2), 5; doi:10.16046/j.cnki.issn2096-1472.2022.02.002. (in Chinese)
2. Menglong, W., Yicheng, Y., Lihua, K., et al., Characteristics analysis and situation prediction of production safety accidents in non-coal mining. Resour. Policy, 2023, 83.
3. Wan, J., Shuai, X. H. and Liang, C., Research and Implementation of a Visualization System for Risk Assessment of Natural Disasters in Non-Coal Mines. China Safety Science Journal, 2022, (S1), 123–129. (in Chinese)
4. Liu, Y., Yan, W., Gao, F., et al., Empirical study on safety performance evaluation of non-coal underground mines. J. Phys. Conf. Ser., 2025, 2969(1), 012013.
5. Liu, Y., Yan, W., Gao, F., et al., Empirical study on safety performance evaluation of non-coal underground mines. J. Phys.: Conf. Ser., 2025, 2969(1), 012013.
6. Wu, M., Ye, Y., Ke, L., et al., Characteristics analysis and situation prediction of production safety accidents in non-coal mining. Resour. Policy,2023,83; doi:10.1016/j.resourpol.2023.

103745.
7. Krishna, K. S., Marine geophysical research in India-new challenges. Curr. Sci., 2021, (9), 121.
8. Byungkyu, J., Hoyoung, J., Seungbeom, C., et al., Assessment of subsidence hazard in abandoned mine area using strength reduction method. KSCE J. Civ. Eng., 2022,26(10),4338–4358.
9. Zhang, Y., Comparative Analysis of Safety Production Conditions in Coal and Non-Coal Mines. China Mining Magazine, 2022, 31(12), 6–8; doi:10.12075/j.issn.1004-4051.2022.12. 024. (in Chinese)
10. Hu, P. C., Study on the Issues and Countermeasures for the Management of Goafs in Underground Mining of Non-Coal Mines. China Science and Technology Journal Database (Industry A), 2023 [No pagination]. (in Chinese)
11. Deck, O., Verdel, T., Salmon, R., Vulnerability assessment of mining subsidence hazards. Risk Anal., 2009, 29(10), 1381–1394; doi:10.1111/j.1539-6924.2009.01238.x.
12. Zhang, X., Zhao, Y., The research of investment risk assessment and management on non-coal mine safety accidents. In: Int. Informatization Eng. Assoc., Atlantis Press. Proc. 2014 2nd Int. Conf. Educ. Technol. Inf. Syst., Humanity Econ. Manag. Coll., China Univ. Geosci., 2014, 84–88.
13. Wu, X., Pan, D. M. and Yu, J. C., Review in the geophysical methods for coalmine goaf prospecting. Progress in Geophysics, 2022, 37(3),1197–1206; doi:10.6038/pg2022GG0128. (in Chinese)
14. Chen, Z. S., Yin, Q. Z., Geng, L. J., Tai, L. X. and Zhang, D. L., Optimization of ground detection method for small closed coal mine. Progress in Geophysics, 2022, 37(1), 367–373. (in Chinese)
15. Cao, S. Y., Sun, Y. G. and Chen, S. Y., Challenges and solutions to high-resolution data processing for seismic exploration. Coal Geology & Exploration, 2023, 51(1), 277–288; doi:10.12363/issn.1001-1986.22.11.0841. (in Chinese)
16. Lahiri, S., Kumar, et al., Gas leakage from palaeogene reservoir in Assam – a geophysical puzzle. Curr. Sci., 2016, 111(7), 1242–1246.
17. Mishra, O. P., Intricacies of the Himalayan seismotectonics and seismogenesis: need for integrated research. Curr. Sci., 2014,106(2),176–187.
18. Rey, J., Mendoza, R., Hidalgo, M. C., et al., A multidisciplinary geophysical approach to characterize a fracture zone: the southern limit of the mining district of Linares-La Carolina, Spain. Geosci., 2024,14(9); doi:10.3390/geosciences14090228.
19. Singh, R. P., Multi geophysical parameters for earthquake forecasting. Curr. Sci., 2013,105 (12), 1657.
20. Ajayakumar, P., Baiju, K. R. and Mahadevan, T. M., Status of Karur-Kambam-Painavu-Trichur shear zone, Southern Granulite Terrain in the context of Late Mesozoic dynamic evolution of Western Ghats: a geophysical-geological perspective. Curr. Sci., 2016,111(11), 1847–1853; doi:10.18520/ cs/v111/i11/1847-1853.
21. Yu, C. T., Liu, C. L., Xue, J. J., Zhang, F. M. and Li, Y., Review in the geophysical methods for coalbed methane resources in abandoned coal mines. Journal of Jilin University (Earth Science Edition), 2023,53(6),1991–2005; doi:10.13278/j.cnki.jjuese.20230284.(in Chinese)
22. Lan, Y., Research on the safety situation and countermeasures of the Dabaoshan mine goaf in Guangdong. China Safety Science Journal, 2022, (S1), 159–164. (in Chinese)
23. Ma, G. S., Mapping water-rich goaf utilizing microtremor survey methods. Progress in Geophysics, 2022, 37(3), 1292–1300; doi:10.6038/pg2022FF0329. (in Chinese)
24. George, N. J., Atat, J. G., Udoinyang, I. E., Akpan, A. E. and George, A. M., Geophysical assessment of vulnerability of surficial aquifer in the oil producing localities and riverine areas in the coastal region of Akwa Ibom State, Southern Nigeria. Curr. Sci., 2017,113(3),430–438; doi:10.18520/cs/v113/i03/430-438.
25. Truong, Q. T., Descloitres, M., Ngo, P. T., et al., Investigating aquifer vulnerability in the Saigon River Basin (Vietnam) using time domain electromagnetic soundings (TDEM). J. Hydrol. Reg. Stud., 2025, 58, 102306.
26. Francés, A. P., Ramalho, E. C., Monteiro Santos, F., et al., Contribution of the time domain electromagnetic method to the study of the Kalahari transboundary multilayered aquifer systems in Southern Angola

. Hydrogeol. J., 2024,32,1709–1727; doi:10.1007/s10040-024-02822-x.
27. Gehad, G., Mohammed, T. H., Ahmed, G., et al., Groundwater quality assessment along the West of New Damietta Coastal City of Egypt using an integrated geophysical and hydro chemical approaches. Environ. Earth Sci., 2023, 82(4) [No pagination].
28. Qin, Q. Y., Application of Time-domain Electromagnetic Method in detecting water accumulation in goafs. Coal Science and Technology, 2014, (8), 109–112. (in Chinese)
29. Jiang, Z. H. and Yang, G., Research and application of TEM detection technology for small mine gob area in shallowly-buried and extremely thick seam. *Journal of Mining & Safety Engineering*, 2014, 31(5), 769–774. (in Chinese)
30. Wang, X. P. and Zhang, X. J., Application of Time-domain Electromagnetic Method and controlled-source electromagnetic method in detecting multi-layer water-filled goafs. Coal Technology, 2019, 38(4), 71–74; doi:10.13301/j.cnki.ct.2019.04.026. (in Chinese)
31. Valdés-Moreno, B., De Basabe, J. D. and Pérez-Flores, M. A., Spectral-element modeling of the time-domain electromagnetic field in 3D geophysical anisotropic media. Comput. Geosci., 2025,29(3); doi:10.1007/s10596-024-10335-5.
32. Yu, X., Zhang, P. and Yu, X., A deep learning inversion method for airborne time-domain electromagnetic data using convolutional neural network. Appl. Sci., 2024, 14(19); doi:10.3390/app14198883.
33. Ahmed, A., Aigner, L., Michel, H., et al., Assessing and improving the robustness of Bayesian evidential learning in one dimension for inverting time-domain electromagnetic data: introducing a new threshold procedure .Water, 2024, 16(7), 1056.
34. Xie, H. J., Meng, X. H., Wang, X. W., et al., Additional effects of Time-domain Electromagnetic Method in detecting water-filled goafs in coal mines. Coal Geology & Exploration, 2009, (2), 74–77; doi:10.3969/ j.issn.1001-1986.2009.02.019. (in Chinese)
35. Zhan, W. F., Wang, Q. and Niu, X. C., Time-domain Electromagnetic Method for detecting goafs in coal mines. Coal Science and Technology, 2010, (8), 3–12; CNKI:SUN:MTKJ.0.2010-08-032. (in Chinese)
36. Xie, H., Guo, Y., Li, G., et al., Laterally constrained inversion of time-domain transient electromagnetic data and using it for detecting water-rich zones in coal mines. Mine Water Environ., 2025; doi:10.1007/s10230-025-01036-1.
37. Pal, S. K., Kumar, S., Srivastava, S., et al., Integrated geophysical approach for coal mine fire in Jharia coalfield, India. Res. Sq., 2021-03-22 [Preprint], (Version 1); doi:10.21203/rs.3.rs-302068/v1.
38. Feng, S. J., Yang, Z. J., Li, H. Z., et al., Application of Time-domain Electromagnetic Method in detecting goafs beneath open-pit slopes. Metal Mine, 2012,(6),47–49; doi:10.3969/j.issn.1001-1250.2012.06.013. (in Chinese
39. Liu, S. Q. and Li, J. Z., Application of transient electromagnetic detection technology in water-filled goafs of coal mines.Coal Technology, 2016, 35(6), 149–151; doi:10.13301/j.cnki.ct.2016.06.061. (in Chinese)
40. Niu, H. and Chen, L. C., Research on Time-domain Electromagnetic Method for detecting closely spaced multi-layer goafs. Mining Safety & Environmental Protectio, 2012, 39 (2), 3–9; (in Chinese)
41. Pronenko, V. and Dudkin, F., Electromagnetic system for detection and localization of miners caught in mine accidents. Geosci. Instrum. Method. Data Syst., 2016, 5(2), 561–566.
42. Knight, J. H. and Raiche, A. P., Transient electromagnetic calculation using the Gaver-Stehfest inverse Laplace transform method. Geophysics, 1982,47(1),47–58; doi:10.1190/1.1441280.
43. Chen, J., Gu, Y., Wang, M. H., Chen, W. and Liu, L. G., Application of the generalized finite difference method to three-dimensional transient electromagnetic problems. Eng. Anal. Bound. Elem., 2017, 92(6), 257–266; doi:10.1016/j.enganabound.2017.08.015.
44. Bobrov, N. Yu., Krylov, S. S., Antonov, E. Yu., Shein, A. N. and Smilevets, N. P., Physical and mathematical modeling of transient electromagnetic soundings over salt-dome structures. Russ. Geol. Geophys., 2017, 58(2),209–218; doi:10.1016/j.rgg.2016.03.017